Ultralow-loss silicon waveguide crossing using Bloch modes in index-engineered cascaded multimode-interference couplers

Yang Zhang,[1,3,†] Amir Hosseini,[2,4,†] Xiaochuan Xu,[1] David Kwong,[1] and Ray T. Chen[1,5]

[1]*Department of Electrical and Computer Engineering, The University of Texas at Austin, 10100 Burnet Rd., Austin, Texas 78758, USA*

[2]*Omega Optics, Inc., 10306 Sausalito Dr., Austin, Texas 78759, USA*

[3]*e-mail: yangzhang@utexas.edu*

[4]*e-mail: amirh@utexas.edu*

[5]*e-mail: raychen@uts.cc.utexas.edu*

Received July 17, 2013; accepted August 12, 2013;
posted August 14, 2013 (Doc. ID 194159); published September 10, 2013

We investigate the loss mechanism in three-moded multimode-interference couplers that are the building blocks of a compact and low-loss waveguide crossing structure. Broadband silicon waveguide crossing arrays with <0.01 dB insertion loss per crossing are proposed using cascaded multimode-interference couplers, where lateral subwavelength nanostructures are used to reduce the insertions loss. We design and fabricate a 101 × 101 waveguide crossing array with a pitch of 3.08 μm. Insertion loss of ~0.02 dB per crossing and crosstalk < – 40 dB at 1550 nm operating wavelength and a broad transmission spectrum ranging from 1520 to 1610 nm are experimentally demonstrated.

OCIS codes: (130.3120) Integrated optics devices; (130.2790) Guided waves; (230.7370) Waveguides.
http://dx.doi.org/10.1364/OL.38.003608

Efficient waveguide crossings are required to materialize the full potential of silicon photonics for on-chip optical interconnects. Single-mode silicon waveguide crossings with normal intersections result in more than 1 dB loss and ~ – 10 dB crosstalk due to the high index contrast of the silicon-on-insulator (SOI) platform [1,2]. This issue has been addressed by several groups over the past decade. Subwavelength gratings in silicon waveguides have been used to lower the effective refractive index at the crossing, resulting in insertion loss as low as 0.023 dB and < – 40 dB crosstalk [1]. However, this structure requires ~10 μm long adiabatic tapers to gradually reduce the effective refractive index with near 0.3 dB loss per taper. Also, the reduced effective refractive index (<2) is accompanied by the mode profile extending several micrometers laterally, which in turn increases the waveguide pitch in a cross-grid structure. As another approach, low-Q resonator-based crossings suffer from limited optical bandwidth (10–15 nm) [3]. Vertically integrated silicon nitride waveguides over SOI waveguides have been shown to reduce the crosstalk to < – 44 dB [4]; however, the required fabrication process is more complicated than that of single-layer photonic integrated circuits (PICs).

On the other hand, multimode-interference (MMI)-based crossings with relatively compact sizes (13 μm × 13 μm) have been demonstrated with insertion loss of ~0.2 dB [2,5]. In this type of structure, the self-focusing effect of the MMI is used to form a single image of the MMI input waveguide mode profile at the crossing, thus minimizing the effect of the crossing waveguide on the mode profile. Recently, using 2D finite-difference time-domain (FDTD) simulations, it was theoretically shown that a periodic structure formed by cascading multimode focusing sections can support a low-loss Bloch wave [6]. In addition to the fact that this structure can potentially lower the insertion loss to 0.04 dB per crossing, a waveguide pitch of ~3 μm also enables compact waveguide crossing arrays. In this Letter, we show that a compact periodic structure formed by cascading MMIs with engineered lateral cladding refractive index can lead to less than 0.01 dB loss per crossing, allowing integration of 100 s of waveguide crossings with minimal insertion loss and crosstalk.

The platform is a SOI substrate with a 3 μm thick buried oxide (BOX) layer and 250 nm thick top silicon layer ($n_f = 3.47$). A schematic of the waveguide array crossing structure is shown in Figs. 1(a) and 1(b). This arrayed structure may be thought of as a cascaded MMI-based waveguide crossing shown in Fig. 1(c), in which, according to the self-imaging principle of multimode waveguides, images of the input field are periodically formed along the multimode waveguide. It has been proposed that the multimode waveguide can be crossed by another one at the points where single-fold images are formed [2].

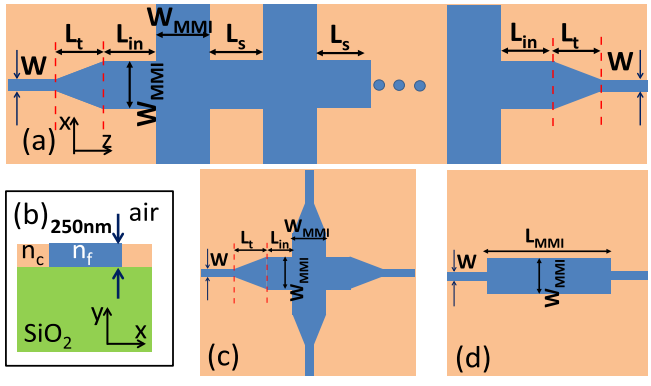

Fig. 1. (a) Top-view schematic of the cascaded MMI-based waveguide crossings. (b) Side view schematic of the waveguide structure with lateral cladding indicated. (c) Single waveguide crossing structure. (d) 1 × 1 MMI.

In order to design a low-loss waveguide crossing array, we first investigate the loss mechanism in the simple 1×1 symmetric MMI structure shown in Fig. 1(d). Similar to a previously reported design [6], here we assume the multimode waveguide width, $W_{\mathrm{MMI}} = 1.2$ μm, and input/output single-mode waveguide width, $W = 0.6$ μm. Note that the MMI region only supports three TE polarized modes. So far, the MMI insertion loss has been explained by the modal phase errors in the multimode waveguide [7–9].

For an ideal self-imaging, it is required that $\beta_{m,\mathrm{ideal}} = \beta_0 - m(m+2)\pi/3L_\pi$, where β_m is the propagation constant of mode m, and L_π is the beat length of the self-imaging process [10]. Following the analysis in [7], one can write

$$\beta_m = \beta_0 \sqrt{1 + \frac{K_{T0}^2 - K_{Tm}^2}{\beta_0}}, \tag{1}$$

where $K_{Tm} = (m+1)\pi/W_{em}$ is the transverse wave number of mode m, and W_{em} is the effective width of the MMI for the mth mode. The modal phase error is given as $\Delta\varphi_m = L_{\mathrm{MMI}}\Delta\beta_m = L_{\mathrm{MMI}}(\beta_m - \beta_{m,\mathrm{ideal}})$, where L_{MMI} is the MMI length. It has been shown that the lateral cladding index (n_c) [see Fig. 1(b)] can be tuned to minimize $\Delta\varphi_m$ for a few numbers of dominant modes. Particularly, at the N-folding imaging length, $\Delta\varphi_m$ is given as

$$\Delta\varphi_m \approx (P/4)\frac{\lambda_0^2(m+1)^4\pi}{2Nn_f^2W_{e0}^2}\left[\frac{1}{8} - \frac{\lambda_0 n_{f2D}^2}{6\pi W_{e0}(n_{f2D}^2 - n_{c2D}^2)^2}\right], \tag{2}$$

where λ_0 is the optical wavelength and P is the number of self-imaging periods. We added the multiplier $P/4$ to the modal phase error presented in [8], since we have a symmetric interference here (required MMI length is divided by 4 [9]), and $P = 2$ in the MMI crossing structure. Also, we note that $n_{f2D} = 2.9$ and n_{c2D} are the effective refractive indices of the fundamental mode of infinite slab waveguides with the same thickness as the MMI (250 nm) and core refractive indices of n_f and n_c, respectively.

While tuning the lateral cladding index (n_c) is generally applicable to MMIs that support several modes in their multimode region, we notice that the multimode waveguide shown in Fig. 1(d) only supports three modes (zeroth, first, and second), among which the odd first-order mode is not excited to due to the symmetry of the structure. That leaves only two modes ($m = 0$ and $m = 2$), for which the self-imaging condition is simply reduced to

$$\beta_0 - \beta_2 = 2\pi n/L_{\mathrm{MMI}}, \qquad n:\mathrm{integer}. \tag{3}$$

One notes that for any W_{MMI} and n_c, as long as only the zeroth and the second modes are excited, there is always an MMI length for which this condition can be perfectly satisfied. In other words, the remaining phase error ($\Delta\varphi_2$) can be in theory completely eliminated by tuning L_{MMI}.

In order to confirm this observation, we simulate different 1×1 MMI structures shown in Figs. 2(a)–2(c) using 3D PhotonDesign FIMMPROP, an eigenmode decomposition-based simulator. Linear tapers ($L_t = 1$ μm) are used in Figs. 2(b) and 2(c) for high transmissions, as

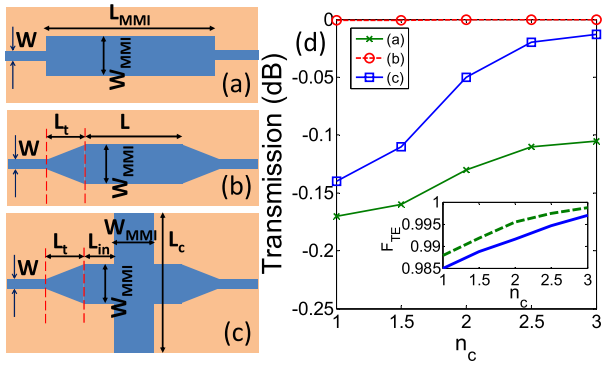

Fig. 2. Schematics of simulated structures. (a) 1×1 MMI with single-mode access waveguides. (b) 1×1 MMI with tapered input output transitions. (c) MMI waveguide crossing using 1×1 MMI with tapered input output transition. (d) Simulated transmission versus lateral cladding index (n_c) for the structure in (a)–(c). The inset of (d) shows the TE fraction versus n_c for the fundamental mode in the single-mode access waveguide (width = 0.6 μm, solid blue curve) and the second-order mode in the MMI region (width = 1.2 μm, dashed green line).

suggested by Chen and Chiu [5]. In each case, we sweep the MMI lengths, L_{MMI}, L, and L_{in}, for MMIs shown in Figs. 2(a)–2(c), respectively, and find the maximum transmission. Figure 2(c) shows optical transmission as a function of n_c. As n_c increases, the transmission improves in all cases. Interestingly, the 1×1 MMI with tapers and without crossing is essentially lossless, and the 1×1 MMI without tapers has the worst performance. Since the modal phase errors are not applicable in any of these cases, we need to consider a different loss mechanism.

In the structure shown in Fig. 2(a), we note that the fundamental mode in the single-mode access waveguide, and the second-order mode in the multimode region, are both quasi-TE modes with a considerable amount of TM polarization (~1.5%) for $n_c = 1$ as shown in the inset of Fig. 2(d). Here, the TE (TM) fraction is the fraction of the Poynting vector with horizontal (vertical) electric field

$$F_{\mathrm{TE}} = \frac{\int E_x H_y \mathrm{d}s}{\int P_z \mathrm{d}s}. \tag{4}$$

As n_c increases, both of these modes become essentially completely TE ($F_{\mathrm{TE}} \sim 100\%$) and the power transmission between the two waveguides improves at the input and output. The tapers help improve the power transmission by avoiding sharp transitions and by reducing the portion of the power in the second-order mode in the multimode region [5].

Similarly, when we compare the tapered MMIs with and without waveguide crossings, we note that the crossing section is much wider compared to the MMI width ($L_c \gg W_{\mathrm{MMI}}$); this section can be thought of as a slab waveguide that supports pure TE modes. When n_c increases from 1 to 2.5, the two excited modes in the MMI region also become nearly pure TE and the power transmission between the two sections increases.

Thus, we conclude that the main loss in the three-moded MMI structures is due to coupling loss at sharp transitions and not due to modal phase errors. We also

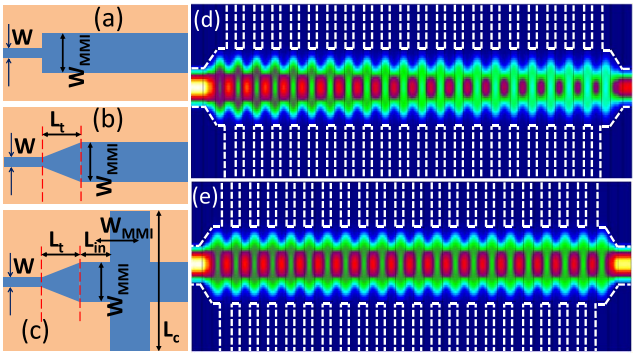

Fig. 3. (a)–(c) Simulated structures for investigation of coupling efficiencies into the 1×1 MMI shown in Figs. 2(a)–2(c). (d), (e) Simulated waveguide crossing arrays for (d) $n_c = 1$, $L_{\text{in}} = 1.35$ μm, and $L_s = 1.04$ μm and (e) $n_c = 2.5$, $L_{\text{in}} = 2.27$ μm, and $L_s = 1.88$ μm.

simulate the structures shown in Figs. 3(a)–3(c) to support this claim. Table 1 depicts the modal field excitation coefficients, c_m, at the outputs (right sides) of the structures shown in Figs. 3(a)–3(c). c_m values are normalized with respect to the input power and are calculated using overlap integrals [10].

One notes that the power transmission from the input single-mode waveguide into the multimode region has about 2% loss in the 1×1 MMI with $n_c = 1$ and without the input taper. This loss is reduced to less than 1% when n_c is increased to 2.5. Adding the input taper makes the coupling from the single-mode input into the multimode waveguide nearly lossless regardless of n_c. Inserting the waveguide crossing section introduces some loss due to sharp transitions between the waveguide sections, where one side supports a quasi-TE mode with a significant TM fraction. Increasing n_c reduces the TM fraction to 0 and increases the overall power transmitted into the supported modes at the output.

Thus, for a large number of waveguide crossings it is imperative to increase the n_c to at least 2.5, where the curve of optical power transmission versus n_c reaches the point of diminishing returns. We simulate the structure shown in Fig. 1(a). Figures 3(d) and 3(e) show the propagation field profiles with 20 crossings, for $n_c = 1$ and $n_c = 2.5$, respectively. The insertion loss is 0.11 and 0.008 dB per crossing in Figs. 1(d) and 1(e), respectively. In these simulations, we maximize the transmission for the structure with 20 crossings, and find $L_{\text{in}} = 1.35$ μm, $L_s = 1.04$ μm for $n_c = 1$ and $L_{\text{in}} = 2.27$ μm, $L_s = 1.88$ μm for $n_c = 2.5$.

We fabricate waveguide arrays normally crossed by other waveguide arrays as shown in Fig. 4(a) using both conventional MMI crossings and index-engineered MMI crossings. In order to implement $n_c > 1$, a subwavelength nanostructure (SWN) is used to engineer the lateral cladding refractive index [8]. The SWN is periodic along the light propagation direction, and its refractive index (n_{SWN}) can be engineered by tuning the filling factor of the air trench inside the SWN, which is defined as the ratio between the air trench width (W) and the SWN period (Λ). We use $\Lambda = 200$ nm for the SWN to fabricate devices with $W = 30$, 40, 50, 60, 70, and 80 nm. The width of the SWN is 200 nm to accommodate the field penetration into the lateral cladding.

The designed structures are fabricated on a SOI wafer using electron beam lithography (EBL) and reactive ion etching (RIE). MMI crossings with and without SWN are used in the cross grids for comparison. Figure 4(b) shows an optical microscope image of the fabricated 101×101 cross grid with index-engineered MMI crossings. Figures 5(a), 5(b) and 5(c), 5(d) show scanning electron microscope (SEM) images of the MMI crossings, with and without SWN, respectively.

TE polarized light from a broadband amplified spontaneous emission light source is coupled in and out of the cross grid using SWN-based grating couplers [11]. The transmissions obtained from the cross grid are normalized to the transmission of a reference waveguide with the same propagation length. We experimentally find that the index-engineered MMI crossing with $W = 50$ nm has the best performance. Figure 6 shows the normalized transmissions of the 101×101 cross grids for a horizontal waveguide in the middle of the grid (the 51st waveguide) with both the index-engineered ($n_c = 2.5$, with SWN) and conventional ($n_c = 1$, no SWN) MMI crossings. The crosstalk measured from a vertical waveguide in the middle of the grid (the 51st waveguide) for an index-engineered structure is also shown in Fig. 6.

The results show that the conventional MMI crossing has an insertion loss of 0.14 dB at 1550 nm operating wavelength, which is comparable to what was demonstrated in [2]. The index-engineered MMI crossing has an insertion loss of 0.019 dB at 1550 nm operating wavelength. The crosstalk signal is below the noise floor of our testing system, so the exact crosstalk cannot be

Table 1. Modal Field Excitation Coefficients c_m in the Three-Mode Sections (Width = W_{MMI}) in Figs. 3(a) and 3(b) and in the Crossing Section (Width = L_c) in Fig. 3(c)[a]

		Fig. 3(a)	Fig. 3(b)	Fig. 3(c)
$n_c = 1$	$\lvert c_0\rvert^2$	0.828	0.936	0.475
	$\lvert c_2\rvert^2$	0.155	0.064	0.326
	$\sum_{m=0}^{M-1} \lvert c_m\rvert^2$	0.983	~1	0.991
$n_c = 2.5$	$\lvert c_0\rvert^2$	0.897	0.949	0.520
	$\lvert c_2\rvert^2$	0.096	0.051	0.312
	$\sum_{m=0}^{M-1} \lvert c_m\rvert^2$	0.993	1	0.998

[a] $L_c = 4$ μm in our FIMMPROP simulations. The total number of modes, M, is 3 at the outputs of the structures in Figs. 3(a) and 3(b). $M = 19$ at the output of the structure in Fig. 3(c).

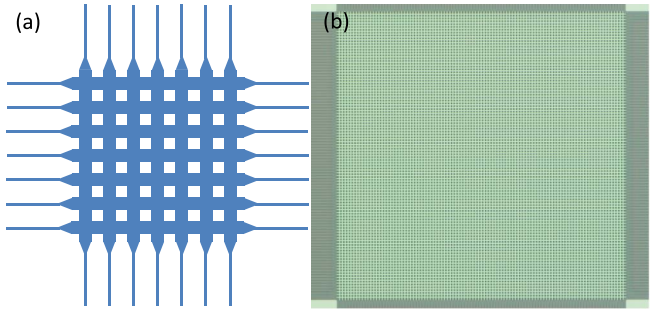

Fig. 4. (a) Schematic of a cross-grid MMI-based waveguide array crossing. A 7×7 cross grid is shown for simplicity. (b) Optical microscope image of the fabricated 101×101 cross grid.

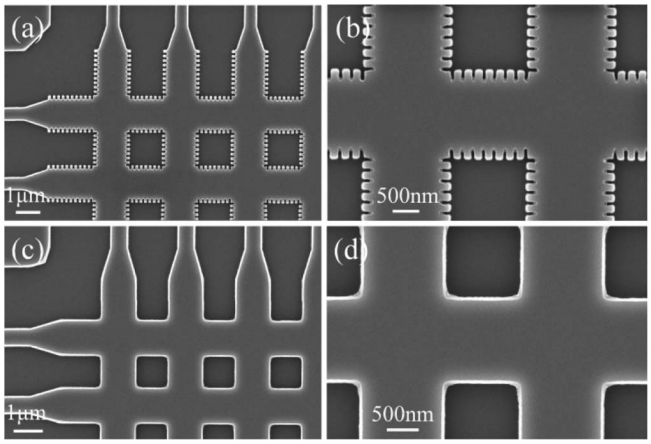

Fig. 5. SEM images of the fabricated waveguide array crossings (a), (b) with and (c), (d) without index engineering of the lateral claddings.

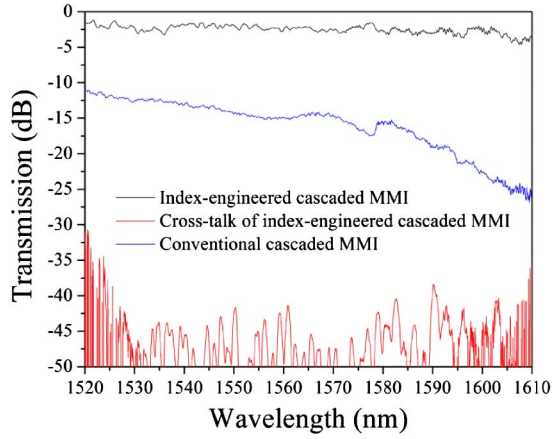

Fig. 6. Measured transmission for 101 cascaded MMI crossings with (black) and without (blue) index engineering, and the crosstalk of index-engineered MMI crossing.

extracted from the transmission. However, the estimated crosstalk is at least below −40 dB over a 1530–1600 nm wavelength range. Besides the ultralow insertion loss and low crosstalk, cascading index-engineered MMI crossings enables a waveguide pitch of 3.08 μm in a cross grid, which is the most compact footprint for a nonresonant crossing to our knowledge.

In summary, while the high index contrast of the SOI platform allows small footprints for photonic devices, it also makes excess loss reduction and crosstalk suppression in waveguide crossings challenging. An ultralow-loss waveguide crossing structure with a waveguide pitch of only 3.08 μm has been demonstrated on the SOI platform. The crossing structure, utilizing cascaded index-engineered MMIs, has an insertion loss of 0.019 dB and crosstalk lower than −40 dB at 1550 nm operating wavelength, and a broad transmission spectrum of more than 90 nm bandwidth.

The authors acknowledge the Multidisciplinary University Research Initiative (MURI) program through the Air Force Office of Scientific Research (AFOSR), contract no. FA 9550-08-1-0394, monitored by Dr. Gernot S. Pomrenke.

†These authors equally contributed to this work.

References

1. P. J. Bock, P. Cheben, J. H. Schmid, J. Lapointe, A. Delâge, D.-X. Xu, S. Janz, A. Densmore, and T. J. Hall, Opt. Express **18**, 16146 (2010).
2. H. Chen and A. W. Poon, IEEE Photon. Technol. Lett. **18**, 2260 (2006).
3. C. Manolatou and H. A. Haus, in *Passive Components for Dense Optical Integration* (Springer, 2002), pp. 97–125.
4. A. M. Jones, C. T. DeRose, A. L. Lentine, D. C. Trotter, A. L. Starbuck, and R. A. Norwood, Opt. Express **21**, 12002 (2013).
5. C.-H. Chen and C.-H. Chiu, IEEE J. Quantum Electron. **46**, 1656 (2010).
6. M. Popovic, E. P. Ippen, and F. Kartner, in *20th Annual Meeting of the IEEE Lasers and Electro-Optics Society* (IEEE, 2007), pp. 56–57.
7. J. Huang, R. Scarmozzino, and R. Osgood, Jr., IEEE Photon. Technol. Lett. **10**, 1292 (1998).
8. A. Ortega-Monux, L. Zavargo-Peche, A. Maese-Novo, I. Molina-Fernández, R. Halir, J. Wanguemert-Perez, P. Cheben, and J. Schmid, IEEE Photon. Technol. Lett. **23**, 1406 (2011).
9. A. Hosseini, D. N. Kwong, Y. Zhang, H. Subbaraman, X. Xu, and R. T. Chen, IEEE J. Sel. Top. Quantum Electron. **17**, 510 (2011).
10. L. B. Soldano and E. C. Pennings, J. Lightwave Technol. **13**, 615 (1995).
11. X. Xu, H. Subbaraman, J. Covey, D. Kwong, A. Hosseini, and R. T. Chen, Appl. Phys. Lett. **101**, 031109 (2012).